CRYSTAL GROWTH & DESIGN

Article

pubs.acs.org/crystal

Novel 3d/4f Metal Organic Networks Containing Co^{II} Chiral Chains

Carlos Cruz,[†,‡] Evgenia Spodine,[†,‡] Andrés Vega,[‡,§] Diego Venegas-Yazigi,[‡,∥] and Verónica Paredes-García*[,‡,§]

[†]Facultad de Ciencias Químicas y Farmacéuticas, Universidad de Chile, Santiago, Chile

[‡]Centro para el Desarrollo de la Nanociencia y Nanotecnología, CEDENNA, Santiago, Chile

[§]Facultad de Ciencias Exactas, Universidad Andres Bello, Santiago, Chile

[∥]Facultad de Química y Biología, Universidad de Santiago de Chile, Santiago, Chile

Supporting Information

ABSTRACT: Novel 3d/4f heterometallic three-dimensional (3D) networks, based on Co^{II}/Gd^{III} cations and imidazole-4,5-dicarboxylic acid (H_3IDC) and oxalate which are acting as main and auxiliary ligand, respectively, were hydro-/solvothermally synthesized using different synthetic strategies. While $[Gd(H_2O)(C_2O_4)Co(IDC)(H_2O)_{1.26}\cdot(CH_3CH_2OH)_{0.74}]\cdot 1.75H_2O$ (**1**) was obtained in a one-pot synthesis, $[Gd(H_2O)Co(HIDC)(C_2O_4)_{1.5}]\cdot 2.65H_2O$ (**2**) was obtained using a Co^{II} complex precursor. Both compounds crystallize in a monoclinic system within the centrosymmetric space group $C2/c$. These structures are characterized by presenting an intricate covalent 3D network. A notable aspect is the fact that in these centrosymmetric structures Co^{II}(IDC/HIDC) moieties are disposed along the networks forming alternate chiral chains, Λ and Δ. From a magnetic point of view, both (**1**) and (**2**) have antiferromagnetic interactions, but in (**1**) a magnetic order appears below 8 K, probably as product of uncompensated antiferromagnetic interactions produced by centers with different spin values. This ferrimagnetic behavior was verified by the hysteresis curve at 1.8 K, and by well-defined maxima, both in the in-phase and out-of-phase *ac* susceptibilities curves. Remarkably, this work reports efficient synthetic methods through which it is possible to generate 3d/4f networks, these being scarce in the literature.

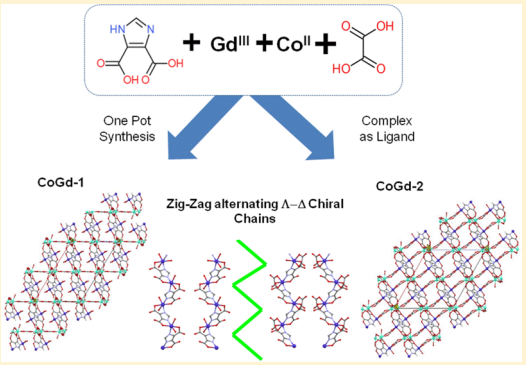

INTRODUCTION

In the last few years, research based on metal−organic frameworks (MOF) has been associated not only with a wide range of structures and interesting topologies that can be obtained, but also with applications of these systems in catalysis,[1,2] gas absorption,[3,4] sensors,[5,6] luminiscence[7] and magnetism[8,9] among others. Clearly, the properties of MOFs depend on the electronic and chemical characteristics of each constituent and to the multiple network interactions. While the metallic cations are relevant for most of the observed properties, the organic ligands are important in the dimensionality reached by the MOFs and in the interaction they produce between the metallic centers.[10−12]

At the present, the reported MOFs are homometallic systems formed by 3d cations, which are assembled by one or more bridging ligands, the MOFs based on 4f cations being more scarce. Recently, structural studies of 3d/4f heterometallic MOFs have gained much attention due to the different coordination geometries of the metal centers. This fact not only permits more interesting structures to be obtained but also different properties compared with those of homometallic MOFs. Although 3d/4f heterometallic MOFs are interesting for heterogeneous catalysts[13] and sensors,[14] in the field of magnetism the presence of interactions between different spin carriers makes this type of MOFs very attractive to investigate.[15,16]

On the other hand, from a synthetic point of view the preparation of 3d/4f heterometllic MOFs is a challenge for the researchers because it is necessary to combine and to control both the variety and high coordination numbers of the 4f cations with the competition of the 3d and 4f cations for a same type of ligand. These facts make the products completely unpredictable.[17] Normally, two synthetic strategies can be adopted. One of them, considers the self-assembly of the 3d and 4f cations with a multifunctional ligand containing for example N and O as donor atoms. Thereby, if the HSAB theory[18] is considered, the coordination of 4f cations will be to sites rich in O atoms, and that of the 3d cations, with lower hardness, toward both N and O atoms.[19] The other option considers several reaction steps. In a first step the synthesis of a simple 3d coordination compound using a N,O-ligand is done. In a second step, the complex precursor rich in O atoms is used to coordinate the 4f cations.

Received: December 30, 2015
Revised: February 22, 2016
Published: February 24, 2016

DOI: 10.1021/acs.cgd.5b01843
Cryst. Growth Des. 2016, 16, 2173−2182

Taking into account the facts given in the above paragraph, imidazole-4,5-dicarboxylic acid (H_3IDC) can be considered as a good candidate to obtain 3d/4f heterometallic MOFs, because the imidazole ring has N donor atoms available to coordinate 3d cations and also two carboxylates groups which can anchor 4f cations.[20] Furthermore, the presence of the carboxylates groups and the different deprotonated species, which can be obtained depending on the synthetic conditions, makes the H_3IDC a very versatile ligand due to the multiple coordination modes. Additionally, the use of some auxiliary ligand such as sulfate,[14−21] acetate,[22] or oxalate[23] is common in the synthesis of MOFs because it permits enhancement of the complexity of the network and also completion of the coordination sphere of the 4f cations.

In this work, we are reporting two new 3d/4f heterometallic MOFs based on Co^{II}, Gd^{III} and imidazole-4,5-dicarboxylic acid and oxalate, these acting as main and auxiliary ligand, respectively. Both compounds were obtained using different synthetic strategies. While $[Gd(H_2O)(C_2O_4)Co(IDC)(H_2O)_{1.26}(CH_3CH_2OH)_{0.74}]\cdot 1.75H_2O$ (**1**) was obtained in a one-pot synthesis, $[Gd(H_2O)Co(HIDC)(C_2O_4)_{1.5}]\cdot 2.65H_2O$ (**2**) was obtained using a Co^{II} complex precursor. Both 3d/4f heterometallic MOFs were characterized from a structural and magnetic point of view.

EXPERIMENTAL SECTION

All reagents and solvents used to obtain (**1**) and (**2**) were of p.a. quality and used without any previous purification process.

$[Gd(H_2O)(C_2O_4)Co(IDC)(H_2O)_{1.26}(CH_3CH_2OH)_{0.74}]\cdot 1.75H_2O$ (1). **1** was obtained by one-pot synthesis from $CoCl_2\cdot 6H_2O$ (0.117 g, 0.50 mmol), Gd_2O_3 (0.045 g, 0.125 mmol), imidazole-4,5-dicarboxylic acid (0.078 g, 0.50 mmol), $H_2C_2O_4\cdot 2H_2O$ (0.063 g, 0.50 mmol), and triethylamine (350 μL, 5.00 mmol). A mixture of 60 mL of H_2O and 5 mL of ethanol was used as solvent. All reagents were placed in a 100 mL Teflon-lined stainless steel autoclave vessel, and the reaction mixture was heated at 165 °C under self-generated pressure for 4 days. After the reaction was slowly cooled down (3 °C/h) to room temperature, pink rhombic crystals were obtained. (yield 59%). Elemental analysis (%): calcd for $C_{8.48}H_{13.46}N_2O_{12.75}CoGd$: C 18.07, H 2.41, N 4.97, found: C 17.91, H 2.38, N 5.05

$[Gd(H_2O)Co(HIDC)(C_2O_4)_{1.5}]\cdot 2.65H_2O$ (2). **2** was obtained in a two-step reaction, using a previously synthesized mononuclear cobalt(II) complex $[Co(H_2IDC)_2(H_2O)_2]$, which acts as a precursor of (**2**). $CoCl_2\cdot 6H_2O$ (0.234 g, 1.00 mmol), imidazole-4,5-dicarboxylic acid (0.313 g, 2.00 mmol), and triethylamine (350 μL, 5.00 mmol) and ethanol were placed in a flask; then the mixture was refluxed for 4 h. Later, (**2**) was obtained mixing the precursor $[Co(H_2IDC)_2(H_2O)_2]$ (0.041 g, 0.10 mmol), $Gd(acac)_3$ (0.069 g, 0.15 mmol), and $H_2C_2O_4\cdot 2H_2O$ (0.050 g, 0.4 mmol) in 6 mL of water and 5 mL of ethanol. The mixture was placed in a 23 mL Teflon-lined stainless steel autoclave vessel and heated at 170 °C under self-generated pressure for 4 days. The reaction mixture was slowly cooled down (3 °C/h) to room temperature; fuchsia rhombic crystals were obtained (yield 30%). Elemental analysis (%): calcd for $C_8H_{9.3}N_2O_{13.65}CoGd$: C 16.92, H 1.65, N 4.93, found: C 16.76, H 1.62, N 5.02.

Single-Crystal X-ray Diffraction Structural Determination of (1) and (2). X-ray diffraction quality single crystals of both compounds were directly picked from the reaction vessel and glued on the tip of a capillary glass using an epoxy resin. Quick scans on the Bruker APEXII diffractometer confirmed excellent crystal quality, and full recording was done for both compounds. Data were reduced by SAINT,[24] and empirical absorption correction were applied using SADABS.[25] Both structures were solved by using XS in the SHELXTL package,[26] completed by Difference Fourier Synthesis, and then refined by using XL within the same package. During the structure completion process for (**1**) some disorder became evident on one of the coordination positions of cobalt. This was modeled considering that the position was occupied by ethanol, in two different conformations, and water. Refinement of the occupancies led to 0.36, 0.38, and 0.26 for each ethanol conformation and the water molecule, as depicted in Scheme 1.

Scheme 1. Scheme Used for Disorder Modeling around the Coordination Sphere of Co^{II} in 1

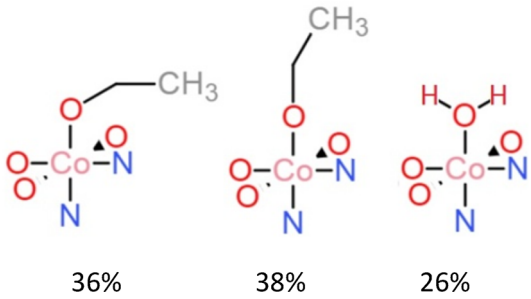

The occupancies of the interstitial water molecules were also refined when partial occupancy was detected. All the refined occupancies were held constant during the last stages of refinement. The H atom positions were calculated after each cycle of refinement using a riding model, with C−H = 0.95 Å (aromatic) or 0.98 Å (methyl). $U_{iso}(H)$ values were set at $1.5U_{eq}(C)$ for methyl groups or at $1.2U_{eq}(C)$ otherwise. The hydrogen atom for HIDC was located in the Difference Fourier map and then refined with the O−H distance restricted to be 0.85 Å. The hydrogen atoms on the water molecules were not located, but were included in the reported formula of the compound. Additional data concerning the crystals and the refinement parameters are detailed in Table S1 in Supporting Information.

Magnetic Susceptibility. Magnetic measurements were carried out using a Quantum Design Dynacool Physical Properties Measurement System (PPMS) equipped with a vibrating sample magnetometer (VSM). The *dc* data were collected under external applied fields of 0.05, 0.1, 0.25, 0.5, 1.0, and 10.0 kOe in the 1.8−300 K temperature range. Diamagnetic corrections (estimated from Pascal constants) were taken into account.[27] Magnetization measurements were performed between −90 and +90 kOe at temperatures varying from 1.8 to 15 K. The dynamic *ac* susceptibility data were collected in the 3.5−12 K range with an applied alternating field of 5 Oe, at frequencies between 134 and 1000 Hz.

Spectroscopic Measurements. FTIR spectra were recorded on a PerkinElmer BX-II spectrophotometer in the 4000−400 cm^{-1} range, using KBr pellets. UV−vis spectra were obtained on a PerkinElmer Lambda 1050 spectrophotometer UV/vis/NIR, equipped with a PerkinElmer 150 mm InGaAs Integrating sphere. The measurements were carried out in the 200−2000 nm range using the solid sample without any support.

RESULTS AND DISCUSSION

Synthesis and Spectroscopic Measurements. From a synthetic point of view, it is important to remark that two 3d/4f tridimensional networks containing Co^{II} and Gd^{III} were obtained, using different synthetic approaches. Although $[Gd(H_2O)(C_2O_4)Co(IDC)(H_2O)_{1.26}(CH_3CH_2OH)_{0.74}]\cdot 1.75H_2O$ (**1**) and $[Gd(H_2O)Co(HIDC)(C_2O_4)_{1.5}]\cdot 2.65H_2O$ (**2**) have similar organic components (imidazole-4,5-dicarboxylic acid and oxalate), some small but important differences were observed. For example, the different protonation degrees that the ligand H_3IDC can acquire depending on the synthetic conditions permitted isolation of this ligand as IDC^{3-} in (**1**) and as $HIDC^{2-}$ in (**2**). On the other hand, even though the H_3IDC ligand meets all the conditions to bind simultaneously 3d and 4f cations, to incorporate an auxiliary ligand such as the oxalate anions has been also reported to be efficient for the

DOI: 10.1021/acs.cgd.5b01843
Cryst. Growth Des. 2016, 16, 2173−2182

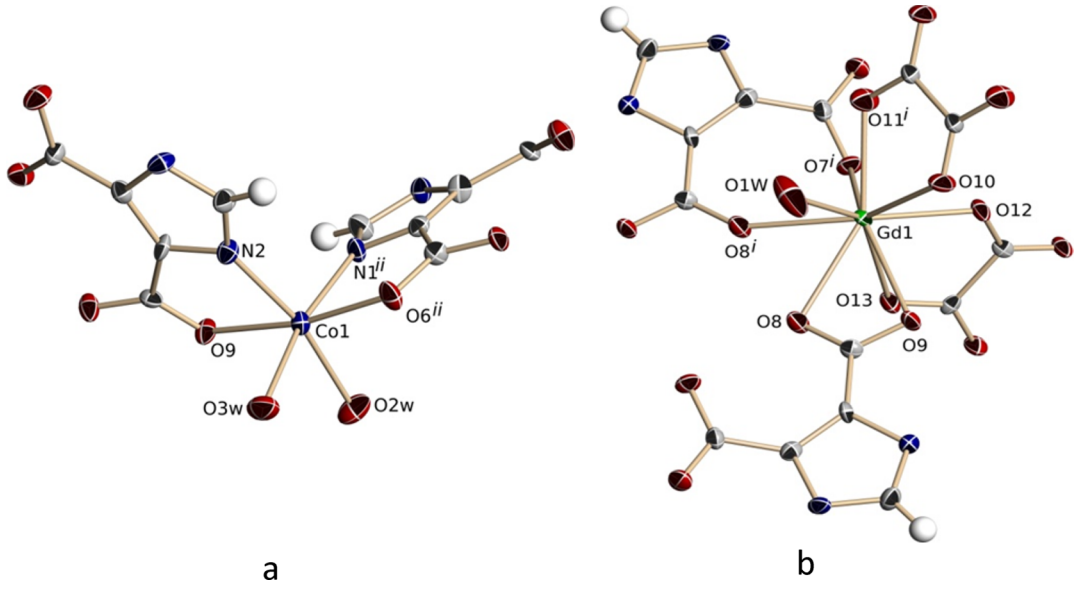

Figure 1. Coordination environment of **1**. (a) Co^{II} and (b) Gd^{III}.

Scheme 2. Coordination Modes of Organic Ligands[a]

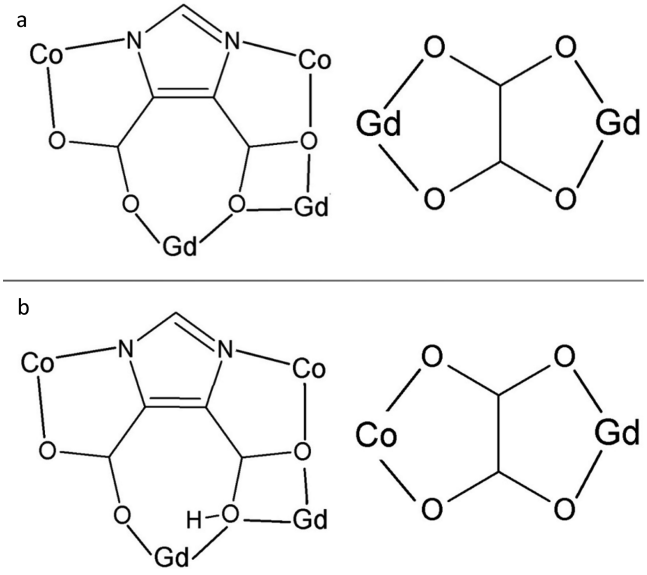

[a](a) IDC^{3-} and oxalate anions in **1**; (b) $HIDC^{2-}$ and oxalate anion in **2**.

generation of 3d/4f-heterometallic compounds. As an example the preparation of $\{[Ln_2(H_2O)_2Zn_4(H_2O)_4(IDC)_4(ox)]_3 \cdot 6H_2O\}_n$ (Ln^{III} = La, Nd, Sm, Eu) and $[Ln_4(H_2O)_4Zn_4(H_2O)_4(IDC)_4(ox)]_3 \cdot 2CH_3OH_3 \cdot 2H_2O$ (Ln^{III} = Eu, Gd, Dy, Ho, Er, Yb, and Lu) can be mentioned.[28] Additionally, another common synthetic strategy to obtain 3d/4f compounds consists of the use of a simple complex species acting as ligand; however this strategy is used less often to obtain extended networks. The work of Yao et al.,[29] reports that the use of a previously synthesized Co^{II} precursor, $[Co(3,5\text{-pdc})(H_2O)_5] \cdot H_2O$ (pdc = pyridine dicarboxylic acid) permits to generate extended networks. Thus, when the complex precursor of Co^{II} is mixed with Gd^{III} and La^{III} under hydrothermal conditions a bidimensional network of $[LnCo(pdc)_2(Hpdc)(H_2O)_7] \cdot H_2O$ (Ln = Gd^{III}, La^{III}) can be obtained.[29]

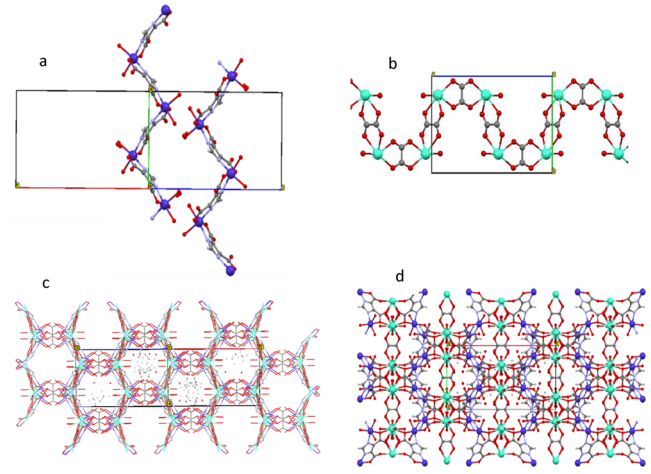

Figure 2. Different structural views of **1**. (a) $[Co(IDC)(H_2O)_{1,26}(CH_3CH_2OH)_{0,74}]_n$ chains along [100]. (b) $[Gd(H_2O)(C_2O_4)]_n$ chain along [010] (c) Ethanol and water molecules in pseudo pores. (d) Schematic view of the crystal lattice. Green: gadolinium cations; blue: cobalt cations.

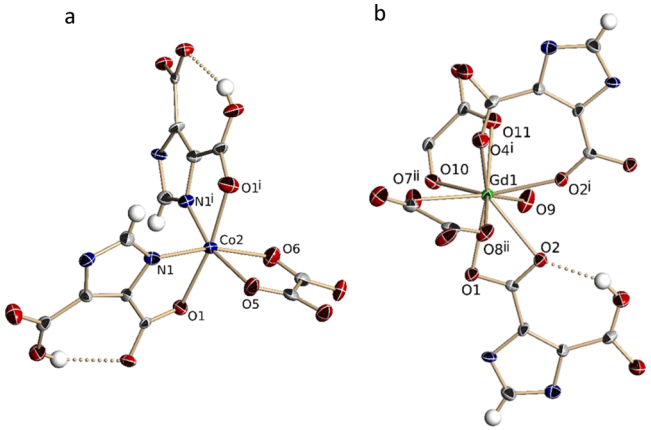

Figure 3. Coordination environment of **2**. (a) Co^{II} and (b) Gd^{III}.

DOI: 10.1021/acs.cgd.5b01843
Cryst. Growth Des. 2016, 16, 2173−2182

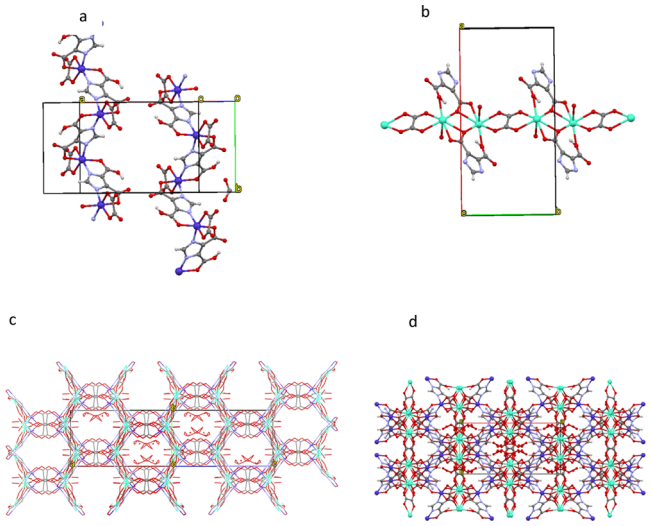

Figure 4. Different structural views of **2**. (a) $[Co(HIDC)(C_2O_4)]_n$ chains along [100]; (b) $[Gd_2(H_2O)_2(HIDC)_2]_n$ chains along [010]; (c) water molecules in pseudo pores (d) Schematic view of the crystal lattice. Green: gadolinium cations; blue: cobalt cations.

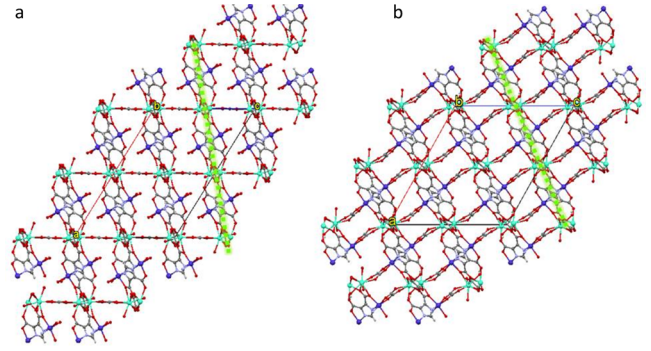

Figure 5. View along [010] axis of extended structure of (a) **1**; (b) **2**. Green: gadolinium cations; blue: cobalt cations.

The above-mentioned synthetic methodologies were used to obtain (**1**) and (**2**) incorporating in both cases, the oxalate as auxiliary ligand and using a mixture of EtOH/water as solvent. However, the synthesis of (**2**) considered a step in which a previously synthesized and characterized mononuclear complex $[Co(H_2IDC)_2(H_2O)_2]$ was used. Also, it is important to remark that if ethanol is not used as solvent only an amorphous phase is obtained, indicating the importance of the role of the used solvent in the crystallization process. Clearly, both synthetic methodologies are effective to obtain 3d/4f-heterometallic networks.

FTIR and UV−vis/NIR spectra of (**1**) and (**2**) are given in the Supplementary Figures S1 and S2, which are also compared with that of the free ligand. FTIR spectra are very similar for (**1**) and (**2**) being dominated by a broad band at 3100−3500 cm^{-1} assigned to the stretching vibrations of water molecules (ν_{O-H}).[30,31] Strong and broad absorption associated with asymmetric ($\nu_{COOasym}$) and symmetric (ν_{COOsym}) vibrations of the carboxylate groups belonging of the oxalate and imidazole-4,5-dicarboxylate ligands appear between 1680 and 1550 cm^{-1} and 1470−1380 cm^{-1}, respectively.[23,30−34] These bands are overlapped with the imidazole ring absorptions ($\nu_{C=C}$ and $\nu_{C=N}$), which are found around 1580−1540 cm^{-1}.[23,32−34] The band associated with the protonated carboxylate should appear

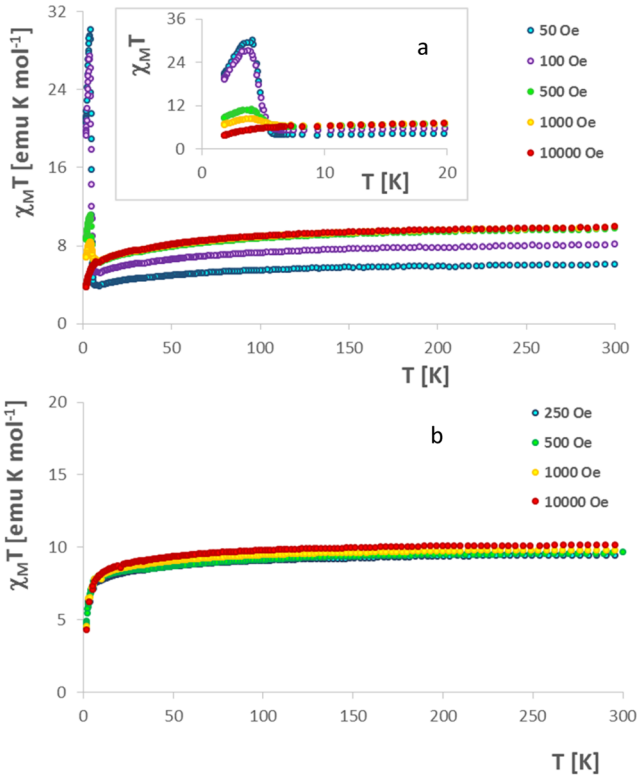

Figure 6. $\chi T(T)$ plots at different applied fields (a) **1**; (b) **2**.

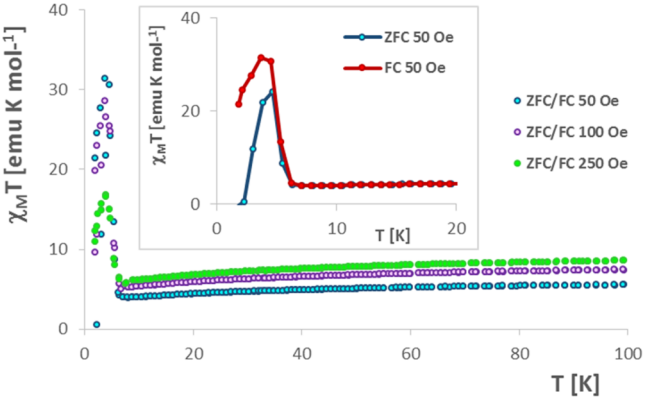

Figure 7. $\chi T(T)$ plots of **1** obtained at 0.05 kOe under ZFC/FC conditions.

at 1700 cm^{-1} but is not observed for (**2**), probably due to the overlapping of the oxalate absorptions.[35,36] Additionally, the band around 3570 cm^{-1}, which is absent in (**2**), may be assigned to the OH vibration belonging to the coordinated ethanol molecules in (**1**).

On the other hand, identical electronic spectra were obtained for (**1**) and (**2**), which are characterized by two strong absorptions at 245 and 300 nm, corresponding to $\pi-\pi^*$ and $n-\pi^*$ transitions of the organic ligands.[30,31,37] The absorptions with lower intensity have been reported in the literature to be d−d transitions of the hexacoordinated Co^{II} cation. While the band in the visible region (570 mn) was assigned to $^4T_1(F) \rightarrow {}^4E_2$, the shoulder at higher energies was assigned to $^4T_1 \rightarrow {}^4A_2$. This assignment was based on the fact that the distorted octahedral configuration causes a low symmetry, and therefore the term $^4T_1(P)$ is split in two components, $^4E_2$ and $^4A_2$.[38] The

DOI: 10.1021/acs.cgd.5b01843
Cryst. Growth Des. 2016, 16, 2173−2182

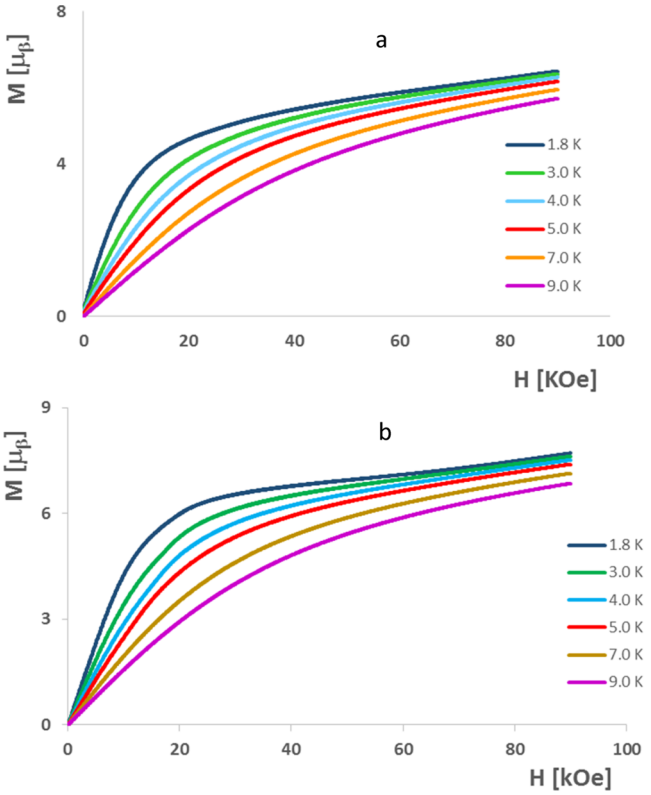

Figure 8. Isothermal magnetizations at different temperatures (a) **1**; (b) **2**.

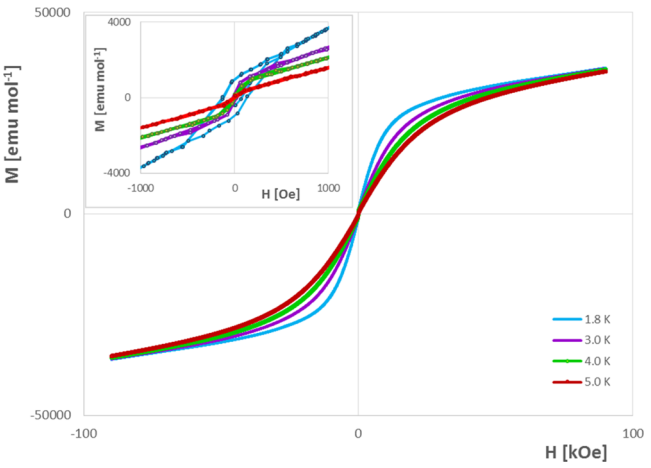

Figure 9. Magnetic hysteresis loop obtained for (**1**) at different temperatures.

last d−d absorption appearing in the NIR zone (1180 nm) was assigned to $^4T_1 \rightarrow {}^4T_2$.[38] The continuous absorption at shorter wavelength (200 nm) was associated with the gadolinium(III) ion, as reported for other compounds containing this lanthanide ion.[39] Excitation at energies associated with each maximum of the absorption spectra were done, but no emission spectra were observed.

Structural Description. *[Gd(H$_2$O)(C$_2$O$_4$)Co(IDC)(H$_2$O)$_{1.26}$·(CH$_3$CH$_2$OH)$_{0.74}$]·1.75H$_2$O* (***1***). The analysis of the single crystal X-ray diffraction for compound (**1**) shows an extended 3D covalent network, with Co^{II} and Gd^{III} centers within the asymmetric unit. The coordination around Co^{II} can be best described as a slightly distorted octahedron with two IDC^{3-} molecules, each one coordinated as a chelating bidentate ligand, water and ethanol molecules in the remaining two positions, as depicted in Figure 1a. The Gd^{III} center is nona-coordinated GdO_9, with nine oxygen atoms from different molecules. The geometry is well described as a nonregular square antiprism.[40] Eight oxygen atoms are provided by carboxylic groups, four from two IDC^{3-} groups and four from two oxalate anions. A water molecule completes the coordination sphere, as shown in Figure 1b.

The coordination spheres of both cations are connected by means of the carboxylate groups. The shortest $Co^{II}\cdots Co^{II}$ (Co1···Co1^{iii}; iii = $-x + 3/2, y - 1/2, -z + 1/2$) distance through an IDC^{3-} anion is 6.361(2) Å as shown in Scheme 2a; it is important to emphasize that Co1 and Co1^{iii} are related by a crystallographic helicoidal 2-fold axis. In the same way, the anion connecting both cobalt cations coordinates to two gadolinium centers at distances of 6.3938(17) Å (Co1···Gd1^{ii}; ii = $-x + 2, -y + 2, -z + 1$), 4.568(2) Å (Co1···Gd1) and 4.2208(14) Å (Gd1···Gd1^{i}; i = $-x + 2, -y + 2, z + 1$). The oxalate anion, $C_2O_4^{2-}$, coordinates exclusively to Gd^{III} centers in a chelating bis-bidentate mode, the two distances being between neighboring Gd^{III} ions of 6.231(2) (Gd1···Gd1^{ii}; ii $-x + 2, -y + 1, -z + 1$) Å and 6.304(2) Å (Gd1···Gd1^{vi}; vi $-x + 2, y, -z + 1/2$). Table S2 shows the most important bond and interatomic distances for (**1**).

The 3D covalent structure of (**1**) can be described in terms of two 1D-substructures, which are mutually perpendicular. The first substructure is formed by chains growing along the *a* axis and is constituted by a zigzag arrangement of Co^{II} diaquo centers connected by IDC^{3-}anions, as depicted in Figure 2a. Since the chain is generated by the two-fold axis, the handedness of each Co^{II} center within it is the same, while the handedness of the nearest neighbor is the opposite. The second substructure is constituted by Gd^{III} aquo centers connected by oxalate anions, defining a ribbon chain along the *b* axis, as depicted in Figure 2b. The assembly of this two perpendicular chains is reached by the coordination of nonbonded carboxylate oxygen atoms of the $[Co(IDC)(H_2O)_{1.26}(CH_3CH_2OH)_{0.74}]_n$ moiety to the gadolinium cation in $[Gd(H_2O)(C_2O_4)]_n$. The obtained 3D covalent lattice is depicted in Figure 2c,d. As a consequence of both chains being mutually perpendicular permits the generation of voids in the structure. As depicted in Figure 2c, elongated cavities are formed, being partially occupied by solvating water molecules or ethanol.

[Gd(H$_2$O)Co(HIDC)(C$_2$O$_4$)$_{1.5}$]·2.65H$_2$O (***2***). The crystal structure of compound (**2**) also corresponds to a 3D network, where Co^{II} and Gd^{III} centers alternate connected by organic ligands. As depicted in Figure 3a, the coordination sphere around Co^{II} is best described as an axially elongated octahedron. The coordination sites are completed by two chelating *N,O*-$HIDC^{2-}$ anions in trans position, and a chelating oxalate anion. The coordination number of Gd^{III} is also 9 as in (**1**), while the coordination geometry is a capped antiprism.[40] Oxygen atoms complete the coordination sites of the lanthanide ion, giving rise to a GdO_9 moiety. As seen in Figure 3b, two chelating $HIDC^{2-}$ anions (with different coordination modes), two chelating oxalate anions and a water molecule complete the coordination sphere of Gd^{III} in (**2**). The coordination mode of $HIDC^{2-}$ is equivalent to that found in (**1**), as depicted in Scheme 2b (6.4606(18) Å (Co2···Co2^{iii}; iii = $-x + 3/2, y - 1/2, -z + 1/2$), 6.5626(18) Å (Co2···Gd1^{i}; i = $-x + 2, -y + 2, -z + 1$), 4.6759(16) Å (Co2···Gd1) and 4.2461(11) Å (Gd1···

DOI: 10.1021/acs.cgd.5b01843
Cryst. Growth Des. 2016, 16, 2173−2182

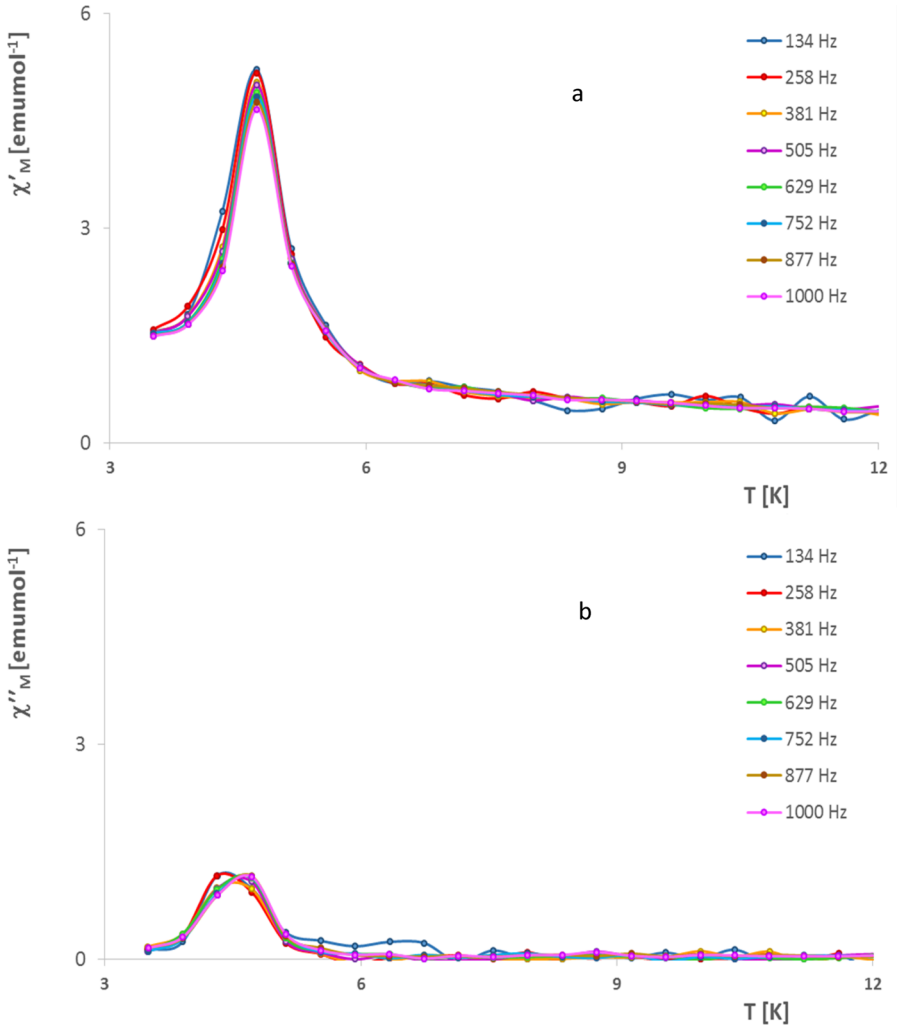

Figure 10. (a) χ' and (b) χ'' plots of **1** obtained at different frequencies.

Gd1^{i}; i = $-x + 2, -y + 2, -z + 1$)). Table S2 shows the most important bond and interatomic distances for (**2**).

In (**2**) not only do Gd^{III}–Gd^{III} oxalate chelating bis-bidentate bridges exist, with a 6.358(1) Å distance (Gd1···Gd1^{v}; v = $x - 2, -y, 1 - z$), but also Co^{II}–Gd^{III} oxalate bridges exist with a length of 5.7988(19) Å (Co2···Gd1^{vi}; vi = $-x + 2, y, -z + 1/2$). Similarly to (**1**), the crystal structure of (**2**) reveals a 3D covalent network, which can also be considered as constituted by two 1D chains. Cobalt(II) O,O′-oxalate units are connected through $HIDC^{2-}$ anions, defining a 1D chain along the *a* axis. Similarly to (**1**), the handedness of each Co^{II} center within each chain is the same, while it must be opposite for the nearest vicinal chains. In the same way Gd^{III} tetraaquobisHIDC dimers are connected through oxalate bridges, defining a 1D chain along the *b* cell axis, as shown in Figure 4.

It is important to take into consideration the great variety of coordination modes with which the H_3IDC ligand can bind to the metal centers, as a result not only of the presence of different functional organic groups but also for the different protonation degrees that the ligand can acquire (H_2IDC^-, $HIDC^{2-}$, IDC^{3-}). Although the adjacent carboxylate groups (in the 4 and 5 positions) may coordinate together with the nitrogen atoms to generate five- or seven-membered rings, in the case of (**1**) and (**2**) the ligand which is present as IDC^{3-} and $HIDC^{2-}$, respectively, interacts through the oxygen atoms with the gadolinium cations. This fact clearly corroborates the preference of the lanthanide ions for the oxygen atoms.

Additionally, IDC^{3-} and $HIDC^{2-}$ forms are the most common species that can be found in heterometallic compounds, $HIDC^{2-}$ being the anion generated by the deprotonation of both carboxylic acid groups. Feng et al.[41] report a family of 3D networks based on Zn_2Ln_2 moieties with Ln = Sm, Eu, Gd, Tb, Dy. The coordination polymers were synthesized with an analogous ligand of H_3IDC, 1*H*-2-methyl-4,5-imidazole-dicarboxylic acid (H_3mIDC), $HmIDC^{2-}$ and $mIDC^{3-}$ species also being present in the reported compounds. Both species have coordination modes similar to those reported in this work, but the $HmIDC^{2-}$ ligand is generated by the deprotonation of two carboxylic acid groups. The $HIDC^{2-}$ species found in (**2**), where the N-imidazole and only one carboxylic acid group are deprotonated, is not common in herterometallic coordination polymers. These deprotonated species have been previously reported for Ni^{II} homonuclear clusters.[42]

Another interesting point is the fact that in both compounds **1** and **2** the chiral chains are formed by $[Co(IDC)(H_2O)_{1.26}(CH_3CH_2OH)_{0.74}]_n$ and $[Co(HIDC)(C_2O_4)]_n$ fragments. However, this chiral property is not transferred to the crystalline structure, as a consequence of the alternating Δ and Λ order of the chains. Although it is not common that

DOI: 10.1021/acs.cgd.5b01843
Cryst. Growth Des. 2016, 16, 2173−2182

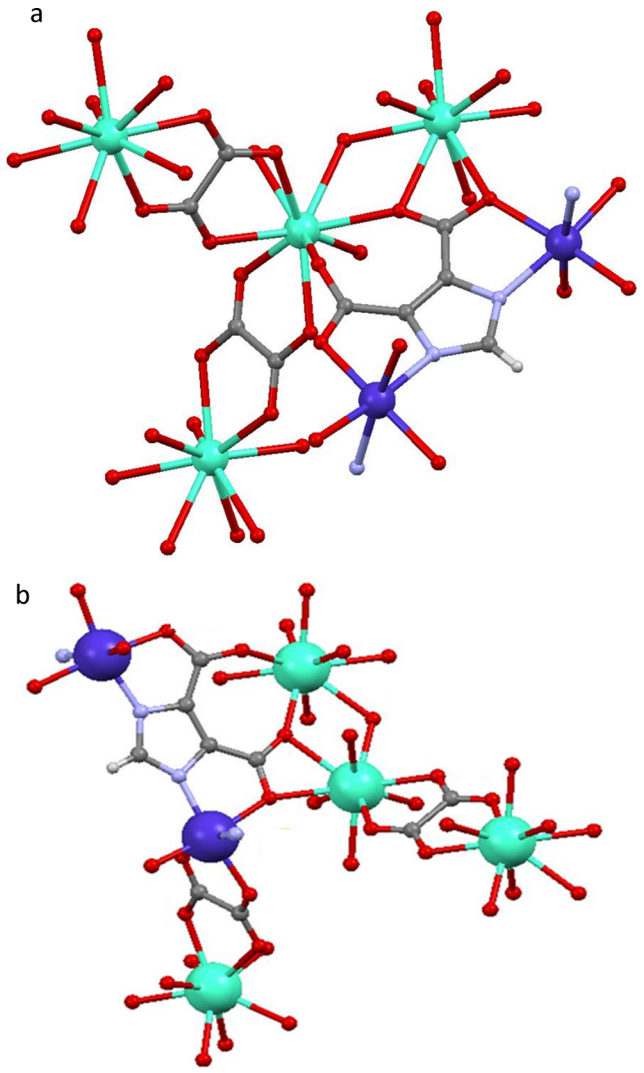

Figure 11. Magnetic exchange pathways that can be found in both 3D coordination polymers.

chiral chains are formed in an achiral reaction media,[43−49] the ligand H_3IDC has been previously reported as forming helical chiral chains. Lu et al.[50] report three isomorphic 2D coordination polymers of $[M(HIDC)(H_2O)(prz)_{0.5}]_n$ (M = Fe^{II} ; Mn^{II}; Cd^{II} ; prz = piperazine) in which the μ^2-$HIDC^{2-}$ ligand alternately bridges the M^{II} cations thus forming right- or left-handed helical chains of $[MHIDC]_n$, which are bridged by prz molecules, and generating a 2D framework. Therefore, considering that in the present work the reagents are achiral, the handedness of the chain can arise both from the coordination capabilities of the H_3IDC ligand and the spatial requirements of the different fragments.[51]

On the other hand, the projection of **1** and **2** along the *b* axis (Figure 5) permits identification of in both cases the same fragment $[Gd(H_2O)Co(HIDC/IDC)(C_2O_4)_{0.5}]^{2+}$, described as parallel sheets. The main difference between both structures is the connection between these sheets. While in (**1**) each sheet is connected through an oxalate ligand, which acts as a bridge between two Gd^{III} ions, in (**2**) the oxalate coordinated to the Co^{II} centers connects the sheets through a Co−ox−Gd bond. Furthermore, the O−C−C−O torsion angle of oxalate ligands binding the $[Gd(H_2O)Co(HIDC)(C_2O_4)_{0.5}]^{2+}$ sheets has a value of 174.66° in (**1**), and 172.63° and 173.72° in (**2**).

Another difference between both structures is the fact that in (**2**) Co^{II} reaches an hexacoordination, binding one oxalate, and two $HIDC^{2-}$ molecules, while in (**1**) it binds to two IDC^{3-} and two water/ethanol molecules. The ethanol molecules in (**1**) are disposed in the pseudo voids generated in the network, with no hydrogen bonds associated with other molecules. This fact is also consistent with the FTIR data and the well-defined absorption observed at 3570 cm^{-1} (absent in **2**), which can be assigned to OH vibration. Additionally, the distortion observed on Co^{II} in both compounds is in agreement with the electronic spectra obtained for (**1**) and (**2**). Finally, although the literature has report of many compounds based on H_3IDC ligand and 3d or 4f metal ions, references including both Co^{II} and Gd^{III} in the same structure, as is the case of the herein reported structures, are relatively scarce.

Magnetic Properties. Magnetic measurements for compounds (**1**) and (**2**) were performed on polycrystalline samples, and the temperature dependence of magnetic susceptibility was studied from 1.8 to 300 K at applied fields of 0.05, 0.1, 0.25, 0.5, 1.0, and 10 kOe. ZFC and FC measurements recorded on (**1**) and (**2**) were also performed at 0.05, 0.1, and 0.25 kOe. Plots of $\chi_M T$ vs T at different applied fields are shown in Figure 6, and plots of χ_M^{-1} vs T are given in Figure S3.

For (**1**) the $\chi_M T$ value at 1 kOe and 300 K is 10.02 emu·K·mol^{-1}, higher than that expected for one Co^{II} and one Gd^{III} ions (9.75 emuK·mol^{-1}; S_{Co} = 3/2, S_{Gd} = 7/2 and g = 2). This product decreases smoothly until 8 K where it reaches a value of 6.48 emu·K·mol^{-1}, indicating that an antiferromagnetic behavior is predominant in this temperature range. From this point an increase of the $\chi_M T$ value is observed, having a maximum around 4 K. At this temperature the intensity of the maximum is dependent on the applied field (inset Figure 6), reaching a value of 30.1 emu·K·mol^{-1} at 0.05 kOe, while for 1 kOe it is 8.3 emu·K·mol^{-1}, being totally suppressed at 10 kOe. Below 4 K the $\chi_M T$ values decreases again, giving values at 1.8 K of 20.5, 19.3, 8.6, 6.8, and 3.8 for 0.05, 0.1, 0.5, 1.0, and 10 kOe, respectively. Clearly the presence of this maximum is indicative of a ferrimagnetic behavior, which becomes predominant in this zone. Moreover, the plot obtained for (**1**) at 10 kOe is notoriously similar to that obtained for (**2**). Compound (**2**) has a $\chi_M T$ value of 10.10 emu·K·mol^{-1} at 1 kOe and 300 K, which is also higher than that expected for a noninteracting couple of Co^{II} and Gd^{III} cations (9.75 emuK·mol^{-1}; S_{Co} = 3/2, S_{Gd} = 7/2 and g = 2). The $\chi_M T$ value gradually decreases to reach a value of 8.1 emu·K·mol^{-1} at 8 K; then a more abrupt decrease is observed until 1.8 K, reaching a value of 4.7 emu·K·mol^{-1} (Figure 6). Clearly, in both compounds a predominant antiferromagnetic coupling can be observed; however a ferrimagnetic behavior becomes evident below 8 K for (**1**). The higher $\chi_M T$ values observed for (**1**) and (**2**) have been associated with orbital contribution of Co^{II} ions, which can be inferred from the plots of magnetization vs H/T, given as Supporting Information (Figure S4). Furthermore, the χ_M^{-1} vs T curves for (**1**) and (**2**) in the high temperature zone (above 50 K) follows the Curie−Weiss law, and the fit of the experimental data gives θ values of −14.1 and −4.2 K for (**1**) and (**2**), respectively. The negative Weiss constant is also indicative that the bulk interaction between the metal centers is antiferromagnetic in nature.

In order to characterize with more detail the magnetic behavior observed at low temperatures for (**1**), zero field cooled (ZFC) and field cooled (FC) magnetic susceptibility and isothermal magnetization measurements were also performed.

DOI: 10.1021/acs.cgd.5b01843
Cryst. Growth Des. 2016, 16, 2173−2182

$\chi_M T$ vs T plot obtained for (**1**) under ZFC/FC conditions at 0.05, 0.1, and 0.25 kOe is given in Figure 7. The data at 0.05 kOe show a complete reversibility until ca. 5 K; from this temperature a significant irreversibility between ZFC and FC measurements is observed. Both curves present a maximum value for $\chi_M T$, being 24.2 emu·K·mol^{-1} at 4.7 K, and 31.4 emu·K·mol^{-1} at 3.7 K, for the ZFC and FC data, respectively. The maximum value of $\chi_M T$ in the ZFC regime is also coincident with the bifurcation temperature; below this maximum the value of $\chi_M T$ decreases, reaching a value of ca. 0 and 21.5 emu·K·mol^{-1} for ZFC and FC, respectively. Literature data report that the presence of a maximum value for $\chi_M T$ at low temperature, and the hysteresis observed in ZFC/FC measurements can been associated with the presence of uncompensated antiferromagnetic interactions.[52,53] Additionally, the reduced magnetization of (**1**) and (**2**) given in Figure 8 permits obtaining a value of 6.4 and 7.7 μ_β respectively, which are lower than 10 μ_β expected for a noninteracting system, formed by one Co^{II} and one Gd^{III} cations with high spin configuration. Isothermal magnetic hysteresis loops ($M(H)$) at different temperatures, near which the magnetic transition was observed, were also performed. Figure 9 shows the M vs H curves indicating that the saturation was not reached even at the maximum applied field at 1.8 K. However, a coercivity of 130 Oe can be detected at 1.8 K, which decreases to 18 Oe at 3K and 8 Oe at 4K, being inexistent at 5 K. Furthermore, a remnant magnetization (M_r) of 395 emu·mol^{-1} was recorded at 1.8 K, decreasing to 173 Oe at 4 K. The presence of initial magnetization and the S-like shape of $M(H)$ loops have been associated with a magnetic transition from a nonmagnetic ground state to a spin-ordered state.[52,54]

To corroborate the existence of a magnetic ordered spin state, alternating current (*ac*) magnetic susceptibility measurements were performed on (**1**) at zero-*dc* field and a 5 Oe oscillating field, in the frequency range of 134 and 1000 Hz. The temperature dependence of both the in-phase (χ'_M) and out-of-phase (χ''_M) susceptibilities exhibits a well-defined maximum at 4.7 K (Figure 10). This fact not only is in agreement with the *dc* susceptibility data, but also confirms the existence of a transition phase in this region. Moreover, it is important to note that the intensity of the *ac* signal is maximum at zero *dc* field, and decreases when the *dc* field is increased, disappearing completely with fields over 250 Oe (Figure S5). Finally, both the in-phase (χ'_M) and out-of-phase (χ''_M) maxima are frequency independent, which can be related to the existence of long-range ordering.[15,53,55]

Generally, magnetostructural correlations are done with the purpose to establish the factors that govern the exchange coupling between the metallic cations. In the case of (**1**) and (**2**) the analyses and interpretation of magnetic properties is not easy, especially if the complexity of these 3d/4f networks are considered. Figure 11 summarizes the magnetic exchange pathways that can be found in both 3D coordination polymers. Subtle but important differences between these two structures are present, which probably are responsible for the different magnetic behaviors observed at low temperature. In both compounds homometallic and heterometallic interactions can be produced between Co···Co, Gd···Gd, and Co···Gd cations, and even though the same chemical bridges are found in (**1**) and (**2**) some differences can be indicated. While (**1**) is characterized by having Gd^{III} cations bridged by oxalate and oxocarboxylate anions, in (**2**) only the oxalate ligand acts as bridge between the 4f cations. Co^{II} cations are linked by the IDC^{3-} or $HIDC^{2-}$ ligand depending on the compound. Moreover, in (**2**) the Co···Gd centers can interact through carboxylate, oxalate, and $HIDC^{2-}$ anions; however, in (**1**) the Co···Gd interaction is produced only through the carboxylate belonging IDC^{3-} ligands. Cai et al.[56] report a framework $[Gd_2Co(HPyIDC)_2(C_2O_4)_2(H_2O)_4]\cdot 4H_2O$ with H_3PyIDC = 2-(pyridine-3-yl)-4,5-imidazoledicarboxylic acid, having similar connections as found in (**1**) and (**2**). The authors also report antiferromagnetic interactions between 300 and 25 K, and ferrimagnetic interactions below 25 K.[56] Additionally, Cañadillas-Delgado et al.[57] report that oxocarboxylate bridges produce weak antiferromagnetic or ferromagnetic interactions between Gd^{III} centers, depending on the Gd−O−Gd angle, pointing out that angles smaller than 110° produce antiferromagnetic interactions. In the case of (**1**) and (**2**) the Gd−O−Gd is 117.5° and 115.9° respectively; therefore ferromagnetic interactions can be expected for this fragment. Additionally, Meng et al.[58] report oxalate-bridged Gd^{III} coordination polymers, having weak antiferromagnetic interactions between the gadolinium centers. Cañadillas-Delagado et al.[59] also indicate that ferromagnetic behavior can be observed in compounds that have a direct interaction among two or more Gd ions through μ-oxo bridges, while the antiferromagnetic behavior is observed when oxalate is also present as bridge, whereas Chen et al.[60] show that *syn-anti* carboxylato bridges easily induce antiferomagnetic interactions, while anti−anti carboxylato bridges mediate ferromagnetic interactions. Clearly, further studies are necessary to understand the intricate magnetic properties of the heterometallic networks, not only as the product of the metallic characteristics of the cations but also due to multiple magnetic pathways through which it is possible to generate the magnetic interaction.

CONCLUSIONS

In summary, two novel 3D networks based on Co^{II} and Gd^{III} were synthesized using different synthetic strategies, $[Gd(H_2O)(C_2O_4)Co(IDC)(H_2O)_{1.26}(CH_3CH_2OH)_{0.74}]\cdot 1.75H_2O$ (**1**) and $[Gd(H_2O)Co(HIDC)(C_2O_4)_{1.5}]\cdot 2.65H_2O$ (**2**). Both heterometallic networks are assembled by the main and auxiliary ligands, imidazole-4,5-dicarboxylate and oxalate, corroborating also that solvothermal synthesis is an efficient method which makes possible beautiful chemical architectures with more than one property, in this case chirality and magnetism.

Although both 3*d*/4f-componds have similar composition and chemical connections some structural and magnetic differences were established. From a structural point of view, the main difference between both networks is related to the fact that in (**1**) $Co^{II}\cdots Gd^{III}$ are bound by only carboxylate groups, while in (**2**) apart from the carboxylate bridges the oxalate ligand also acts as a bridge between these two metallic cations. Notably, in both compounds the cobalt(II) ions form chiral chains, which are disposed along the network in alternating Λ, Δ form.

From a magnetic point of view, antiferromagnetic interaction were established as the main interactions, but in (**1**) a magnetic order appears below 8 K, which probably is produced by uncompensated antiferromagnetic interactions between centers with different spin values. This ferrimagnetic behavior was also verified by the hysteresis observed at 1.8 K, and by presenting a well-defined maximum at 4.7 K, both in the in-phase and out-of-phase *ac* susceptibilities.

DOI: 10.1021/acs.cgd.5b01843
Cryst. Growth Des. 2016, 16, 2173−2182

Finally, the synthetic approach reported in this work can be used to prepare novel transition-lanthanide metal−organic coordination polymers presenting new structures and interesting properties. Further, the data given in this work, make evident the intricate magnetic properties of these heterometallic networks, which are not only the product of the electronic characteristics of the metal centers but also of the multiple exchange pathways. To understand the different magnetic behaviors of (**1**) and (**2**), further studies are necessary.

■ ASSOCIATED CONTENT

Supporting Information

The Supporting Information is available free of charge on the ACS Publications website at DOI: 10.1021/acs.cgd.5b01843.

Crystal data and refinement details; Bond and interatomic distances; FTIR spectra; UV-Vis spectra; χ^{-1} plots; figure of reduced magnetization obtained at different temperatures; $\chi'$and χ'' plots (PDF)

Accession Codes

CCDC 1443830−1443831 contains the supplementary crystallographic data for this paper. These data can be obtained free of charge via www.ccdc.cam.ac.uk/data_request/cif, or by emailing data_request@ccdc.cam.ac.uk, or by contacting The Cambridge Crystallographic Data Centre, 12, Union Road, Cambridge CB2 1EZ, UK; fax: +44 1223 336033.

■ AUTHOR INFORMATION

Corresponding Author

*E-mail: vparedes@unab.cl.

Notes

The authors declare no competing financial interest.

■ ACKNOWLEDGMENTS

The authors acknowledge financial support from FONDECYT 1130643, Programa de Anillos en Ciencia y Tecología Grant ACT1404, CONICYT-FONDEQUIP/PPMS/EQM130086 and LIA-MIF 836 International collaborative project. The authors are also members of CEDENNA, Financiamiento Basal, FB0807. C.C. acknowledges CONICYT Fellowship 2114042.

■ DEDICATION

In memory of Prof. Ramón O. Latorre.

■ REFERENCES

(1) Yoon, M.; Srirambalaji, R.; Kim, K. *Chem. Rev.* **2012**, *112*, 1196−1231.
(2) Corma, A.; García, H.; Llabrés i Xamena, F. X. *Chem. Rev.* **2010**, *110*, 4606−4655.
(3) Mason, J.; Veenstra, M.; Long, J. R. *Chem. Sci.* **2014**, *5*, 32−51.
(4) Li, J. R.; Ma, Y.; McCarthy, M. C.; Sculley, J.; Yu, J.; Jeong, H. K.; Balbuena, P. B.; Zhou, H. C. *Coord. Chem. Rev.* **2011**, *255*, 1791−1823.
(5) Cui, Y.; Chen, B.; Qian, G. *Coord. Chem. Rev.* **2014**, *273−274*, 76−86.
(6) Kreno, L. E.; Leong, K.; Farha, O. K.; Allendorf, M.; Van Duyne, R. P.; Hupp, J. T. *Chem. Rev.* **2012**, *112*, 1105−1125.
(7) Cui, Y.; Yue, Y.; Qian, G.; Chen, B. *Chem. Rev.* **2012**, *112*, 1126−1162.
(8) Roy, S.; Chakraborty, A.; Maji, T. K. *Coord. Chem. Rev.* **2014**, *273−274*, 139−164.
(9) Zhang, W. X.; Liao, P. Q.; Lin, R. L.; Wei, Y. S.; Zeng, M. H.; Chen, X. M. *Coord. Chem. Rev.* **2015**, *293−294*, 263−278.
(10) Li, B.; Chrzanowski, M.; Zhang, Y.; Ma, S. *Coord. Chem. Rev.* **2016**, *307*, 106−129.
(11) Karmakar, A.; Desai, A. V.; Ghosh, S. K. *Coord. Chem. Rev.* **2016**, *307*, 313−341.
(12) Li, J. R.; Sculley, J.; Zhou, H. C. *Chem. Rev.* **2012**, *112*, 869−932.
(13) Yang, T. H.; Silva, A. R.; Shi, F. N. *CrystEngComm* **2015**, *17*, 3852−3858.
(14) Ding, Y. J.; Li, T.; Hong, X. J.; Zhu, L. C.; Cai, Y. P.; Zhu, S. M.; Yu, S. J. *CrystEngComm* **2015**, *17*, 3945−3952.
(15) Andruh, M.; Costes, J. P.; Diaz, C.; Gao, S. *Inorg. Chem.* **2009**, *48*, 3342−3359.
(16) Huang, Y. G.; Jiang, F. L.; Hong, M. C. *Coord. Chem. Rev.* **2009**, *253*, 2814−2834.
(17) Zhang, S.; Cheng, P. *CrystEngComm* **2015**, *17*, 4250−4271.
(18) Pearson, R. G. *J. Am. Chem. Soc.* **1963**, *85*, 3533−3539.
(19) Zhou, Y.; Hong, M.; Wu, X. *Chem. Commun.* **2006**, *2*, 135−143.
(20) Fang, R. Q.; Zhang, X. M. *Inorg. Chem.* **2006**, *45*, 4801−4810.
(21) Zhu, L. C.; Zhao, Y.; Yu, S. J.; Zhao, M. M. *Inorg. Chem. Commun.* **2010**, *13*, 1299−1303.
(22) Zhang, Q.; Zheng, Y. X.; Liu, C. X.; Sun, Y. G.; Gao, E. J. *Inorg. Chem. Commun.* **2009**, *12*, 523−526.
(23) Li, Z. Y.; Dai, J. W.; Qiu, H. H.; Yue, S. T.; Liu, Y. L. *Inorg. Chem. Commun.* **2010**, *13*, 452−455.
(24) *SAINTPLUS*, V6.22; Bruker AXS Inc: Madison, WI, USA, 2000.
(25) *SADABS*, V2.05; Bruker AXS Inc.: Madison, WI, USA, 2001.
(26) Sheldrick, G. M. SHELXL-97, Program for Crystal Structure Refinement; University of Göttingen: Göttingen, Germany, 1997.
(27) Bain, G.; Berry. *J. Chem. Educ.* **2008**, *85*, 532.
(28) Gu, Z. G.; Fang, H. C.; Yin, P. Y.; Tong, L.; Ying, Y.; Hu, S. J.; Li, W. S.; Cai, Y. P. *Cryst. Growth Des.* **2011**, *11*, 2220−2227.
(29) Yao, J. C.; Guo, J. B.; Wang, J. G.; Wang, Y. F.; Zhang, L.; Fan, C. P. *Inorg. Chem. Commun.* **2010**, *13*, 1178−1183.
(30) Xiong, Z.; Yuan, P.; Xie, Z.; Li, G. *Supramol. Chem.* **2014**, *26*, 346−357.
(31) Zhang, Z. C.; Chen, Y. G.; Tang, Q.; Zhang, C. X.; Meng, H. X. *Synth. React. Inorg., Met.-Org., Nano-Met. Chem.* **2014**, *44*, 434−440.
(32) Li, X. X.; Wang, N.; Yue, S. T.; Li, Z. Y.; Wu, H. Y.; Liu, Y. L. *Z. Anorg. Allg. Chem.* **2009**, *635*, 2648−2652.
(33) Zhang, F.; Li, Z.; Ge, T.; Yao, H.; Li, G.; Lu, H.; Zhu, Y. *Inorg. Chem.* **2010**, *49*, 3776−3788.
(34) Li, Z. Y.; Zhang, Z. M.; Dai, J. W.; Huang, H. Z.; Li, X. X.; Yue, S. T.; Liu, Y. L. *J. Mol. Struct.* **2010**, *963*, 50−56.
(35) Wladimirsky, A.; Palacios, D.; D'Antonio, M. C.; Gonzalez-Baró, A. C.; Baran, E. J. *J. Argent. Chem. Soc.* **2011**, *98*, 71−77.
(36) Fujita, J.; Nakamoto, K.; Kobayashi, M. *J. Phys. Chem.* **1957**, *61*, 1014−1015.
(37) Feng, X.; Feng, Y. Q.; Chen, J. J.; Ng, S. W.; Wang, L. Y.; Guo, Y. Z. *Dalton Trans.* **2015**, *44*, 804−816.
(38) Kumar, N.; Kachroo, P. L.; Kant, R. *Transition Met. Chem.* **1979**, *4*, 315−318.
(39) Strasser, A.; Vogler, A. *Inorg. Chim. Acta* **2004**, *357*, 2345−2348.
(40) Llunell, M.; Casanova, D.; Cirera, J.; Bofill, J. M.; Alemany, P.; Alvarez, S.; Pinsky, M.; Avnir, D. SHAPE V2.1 (this program has been developed in the group of Prof. Alvarez at the Universitat de Barcelona and is available from the authors at llunell@qf.ub.es).
(41) Feng, X.; Ma, L. F.; Liu, L.; Wang, L. Y.; Song, H. L.; Xie, S. Y. *Cryst. Growth Des.* **2013**, *13*, 4469−4479.
(42) Liu, Y.; Kravtsov, V.; Walsh, R. D.; Poddar, P.; Srikanth, H.; Eddaoudi, M. *Chem. Commun.* **2004**, 2806−2807.
(43) Pardo, P.; Train, C.; Lescouëzec, R.; Journaux, I.; Pasán, J.; Ruiz-Pérez, C.; Delgado, F.; Ruiz-García, R.; Lloret, F.; Paulsen, C. *Chem. Commun.* **2010**, *46*, 2322−2324.
(44) Mikhalyova, E.; Kolotilov, S.; Cador, O.; Pointillart, F.; Golhen, S.; Ouahab, L.; Pavlishchuk, V. *Inorg. Chim. Acta* **2010**, *363*, 3453−3460.
(45) Ru, J.; Gao, F.; Wu, T.; Yao, M. X.; Li, Y. Z.; Zuo, J. L. *Dalton Trans.* **2014**, *43*, 933−936.
(46) Cheng, L.; Zhang, L.; Gou, S.; Cao, Q.; Wang, J.; Fang, L. *CrystEngComm* **2012**, *14*, 3888−3893.
(47) Pan, C. Y.; Zhong, L. J.; Zhao, F. H.; Luo, Y. Z.; Li, D. G. *Inorg. Chem.* **2015**, *54*, 403−405.

DOI: 10.1021/acs.cgd.5b01843
Cryst. Growth Des. 2016, 16, 2173−2182

(48) Martínez-Lillo, J.; Armentano, D.; Fortea-Pérez, F.; Stiriba, S. E.; De Munno, G.; Lloret, F.; Julve, M.; Faus, J. *Inorg. Chem.* **2015**, *54*, 4594−4596.
(49) Kang, T. T.; Tang, H.; Wei, Y. L.; Zang, S. Q. *Z. Naturforsch., B: J. Chem. Sci* **2013**, *68*, 403−407.
(50) Lu, W. G.; Gu, J. Z.; Jiang, L.; Tan, M. Y.; Lu, T. B. *Cryst. Growth Des.* **2008**, *8*, 192−199.
(51) Yang, H. X.; Jian, S. J.; Liang, Z.; Zhang, J. D.; Meng, X. R. *Inorg. Chem. Commun.* **2015**, *61*, 57−59.
(52) Ahmad, M.; Sharma, M. K.; Das, R.; Poddar, P.; Bharadwaj, P. K. *Cryst. Growth Des.* **2012**, *12*, 1571−1578.
(53) Liu, X.; Qu, X.; Zhang, S.; Ke, H.; Yang, Q.; Shi, Q.; Wei, Q.; Xie, G.; Chen, S. *Inorg. Chem.* **2015**, *54*, 11520−11525.
(54) Li, J.; Li, B.; Huang, P.; Shi, H. Y.; Huang, R. B.; Zheng, L. S.; Tao, J. *Inorg. Chem.* **2013**, *52*, 11573−11579.
(55) Atzori, M.; Benmansour, S.; Mínguez Espallargas, G.; Clemente-León, M.; Abhervé, A.; Gómez-Claramunt, P.; Coronado, E.; Artizzu, F.; Sessini, E.; Deplano, P.; Serpe, A.; Mercuri, M. L.; Gómez Garcia, C. J. *Inorg. Chem.* **2013**, *52*, 10031−10040.
(56) Cai, S. L.; Zheng, S. R.; Wen, Z. Z.; Fan, J.; Wang, N.; Zhang, W. G. *Cryst. Growth Des.* **2012**, *12*, 4441−4449.
(57) Cañadillas-Delgado, L.; Fabelo, O.; Cano, J.; Pasán, J.; Delgado, F. S.; Lloret, F.; Julve, M.; Ruiz-Pérez, C. *CrystEngComm* **2009**, *11*, 2131−2142.
(58) Meng, Y.; Chen, Y. C.; Zhang, Z. M.; Lin, Z. J.; Tong, M. L. *Inorg. Chem.* **2014**, *53*, 9052−9057.
(59) Cañadillas-Delgado, L.; Pasán, P.; Fabelo, O.; Hernández-Molina, M.; Lloret, F.; Julve, M.; Ruiz-Pérez, C. *Inorg. Chem.* **2006**, *45*, 10585−10594.
(60) Chen, Z. L.; Jiang, C. F.; Yan, W. H.; Liang, F. P.; Batten, S. R. *Inorg. Chem.* **2009**, *48*, 4674−4684.

DOI: 10.1021/acs.cgd.5b01843
Cryst. Growth Des. 2016, 16, 2173−2182